UNCONVENTIONAL RESOURCES TECHNOLOGY CONFERENCE
HOSTED BY SPE • AAPG • SEG

URTeC: 2153938

Unconventional Reservoir Model Predictions Using Massively-Parallel GPU Flow-Simulation: Part-1 Bakken Reservoir Characterization Choices and Parameter Testing

J. R. Gilman, M. Uland*, O. Angola, R. Michelena, H. Meng, iReservoir.com Inc. and
K. Esler, K. Mukundakrishnan, V. Natoli, Stone Ridge Technology

Abstract

This paper discusses application of massively-parallel GPU flow-simulation for the Bakken reservoir. Compared to CPU simulation, GPUs allow larger, faster numerical models (10+ million cells). These larger models can retain important details of geologic characterization (fractures+matrix), allow fine gridding for closely spaced and stacked horizontals and allow for more geology and engineering sensitivity analysis in a reduced time frame. This modern GPU formulation applies standard finite volume approaches for full-physics simulation. Multi-million cell simulation models are shown to run at least an order of magnitude faster than current parallel CPU algorithms.

Development of unconventional reservoir play fairways has demonstrated variability in reservoir characteristics and thus variability in well production rates. Predicting unconventional reservoir performance using flow-simulation requires a myriad of characterization choices for geomodel construction while addressing uncertain engineering data, well spacing and completions. Current software/hardware limitations restrict the practical number of simulation what-if cases such as completions, well spacing, matrix and natural fracture characterization. Current unconventional reservoir single/dual-porosity flow-simulation models are upscaled from detailed geomodels and only retain a hundred thousand to a couple million cells with only a few horizontal well pairs. This paper's GPU based workflow allows retention of geomodel and engineering detail in a reduced flow-sim prediction timeframe.

Introduction

Methods for well performance analysis can be broadly classified into two categories, namely, analytical techniques and numerical methods. Analytical methods (decline curve analysis, DCA and rate transient analysis, RTA) are useful for reviewing the performance of a large number of individual wells where there is sufficient production and pressure data, or when one well model needs to be screened to produce "type curves" where there is a large uncertainty in the reservoir constraining data. Such methods are fast and can be used over a large area but are simplistic in the reservoir description and also not predictive for infill well interference details. On the other hand, flow-simulations using numerical methods, allows the incorporation of more complex geologic details including variable natural fracture intensity and additional engineering details such as variable stimulated reservoir volume (SRV) constrained by microseismic. These methods are usually slow for multi-million cell dual-porosity models with run times around several hours to days for a single simulation. Another class of method called the Discrete Fracture Network (DFN) models that are calibrated to well performance can be useful in modeling detailed flows within the fracture networks on a smaller length scale. The DFN methodology can also be useful to define large scale complex fracture networks, which can be upscaled for dual-porosity models for practical large-scale simulation similar to the continuous fracture models (CFM) shown here (Dershowitz, *et. al*. 2000, Gilman, *et. al*. 2011).

For the present study, in order to retain the geologic and engineering details, a full physics numerical simulator built from the ground-up using Graphics Processing Units (GPUs) has been used. GPUs are high-performance many-core processors that can be used to accelerate a wide range of applications, from gaming to engineering. In general, a well-optimized GPU implementation with the use of appropriate scalable algorithms promises much faster run times

compared to a corresponding central processing units (CPU) implementation because of higher memory bandwidth and throughput. The faster GPU run times can even approach those of analytical techniques (e.g. RTA) without sacrificing the details of the model. Such speeds have enabled the exploration of multiple "what-if" cases without having to severely "upscale/ smooth" geomodel with tens of millions of cells for running the flow-simulations.

In this paper, we employ the new GPU simulator to run an industry-scale uncoventional model. The current major economic unconventional plays (Bakken/Three Forks, Eagle Ford, Wolfcamp, Marcellus/Utica) all with different geology and different fluids have similar simulation modeling problems when predicting the multi-pad and infill well performances. Detailed numerical models are required to capture the matrix, natural fracture, and hydro-frac approximations and test the uncertainty in the assumptions. However, traditional CPU-based simulators can take up to several hours to run a single realization of a high-fidelity model. With hundreds of realizations to simulate and analyze, the run times using such simulators can be overwhelming even with a large cluster-based solutions. Drastic simplifications of the model are therefore made to make the uncertainty-based engineering analysis feasible. For example, smaller well groups are often tested numerically and then the results are extrapolated to larger areas. In this paper, we setup and test the GPU simulator using a nine-section (¼ of a township) multi-well, multi-pad Middle Bakken development case. The nine-section flow-simulation model was extracted from a larger area (120 township) Bakken/Three Forks geomodel constructed by using public data. Figure 1 shows the location of the geomodel, the 9 section flow-simulation model relative to local oil production and water-cut, and a nearby Bakken/Three Forks type log.

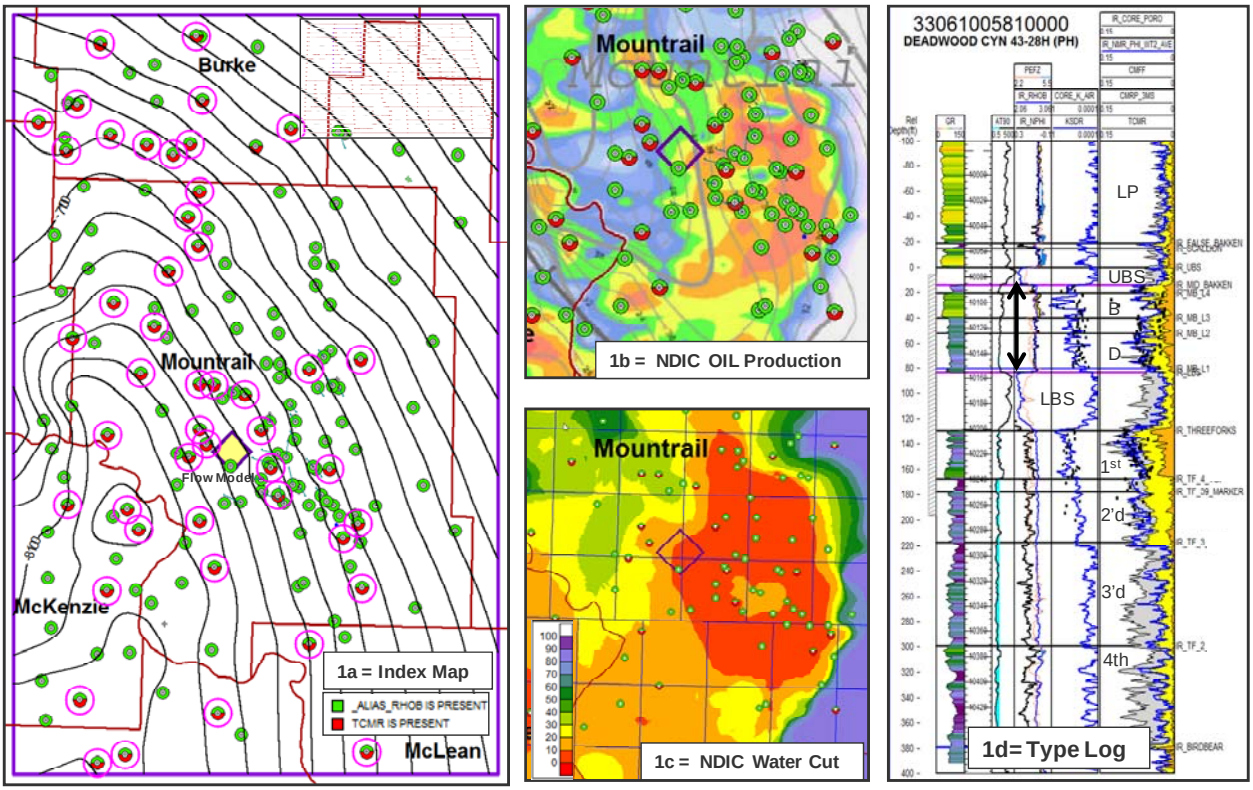

Figure 1. a) 120 township geomodel index map with the vertical well control logs posted, and GPU flow-simulation 9-section model shown in the center as a yellow diamond; b) NDIC 480 day relatively-scaled oil production surrounding the flow-sim model area; c) NDIC relative-scaled water-cut surrounding the flow-sim model area; d) Bakken/Three Forks type log showning the Middle Bakken interval (A,B,C,D,E) that was used in this GPU flow-simulation.

Input Data

The input data used to construct the Bakken through Three Forks static geomodel and initialize the flow-simulation model cases was constructed using public data sources including logs, core, fracture sets, and engineering data from the North Dakota Industrial Commission (NDIC) website, published AAPG data, SPE papers, and university published graduate theses.

Log and core data from older vertical wells and new horizontal pilot holes that were plugged back and kicked off to complete the horizontal wellpath were used to construct the Upper Bakken Shale (UBS) structure grid. In a few areas with sparse vertical data, the UBS true vertical depth tops were picked from the horizontal well curves and were used to constrain the UBS structure grid. The Bakken tops were picked using similar stratigraphy as shown in NDIC report GI-14 (LeFever, 2005).

Most of the recent log data (since 2010) is available at NDIC both as raster files and digital LAS curves. Selected resistivity, gamma ray, neutron, density, sonic curves for the older vertical wells with just raster logs and some of the newer wells with only color rasters were digitized from the lower Lodgepole to the top of the Birdbear or TD, whichever came first. This digital log data set was used in cross-section to verify tops or add missing ones.

The NDIC scanned wells files contain 52 wells with Bakken and/or Three Forks core analysis in the geomodel area. Both rotary sidewall core and conventional core had core plug analysis and some compaction data run at different net confining stress (NCS). Older cores were taken with water base mud (WBM) and most of the newer Bakken and Three Forks cores were taken with oil base mud (OBM). The OBM core data (38 wells) is useful to approximate irreducible water saturation (S_{wi}) in the dry oil production areas and to estimate the total water saturation (SWT) as $S_{wi}+S_{wm}$ in areas that have a stabilized producing water cut. A few well files report core XRD results to help verify lithology.

The NDIC data set includes a significant set of modern specialty logs including nuclear magnetic resonance (NMR) logs (both as CMR and MRIL), estimated lithology logs (ECS), and elastic property logs (Dipole Sonics and Sonic Scanners). The NMR total porosity (TCMR) is a good approximation to the reported core porosity (helium) and is available on 47 wells in the geomodel area. The NMR estimated permeability logs as Ktim and KSDR was available on 39 wells in the geomodel area. The fast azimuth orientation for the dipoles was useful to help verify the N45E average direction for the reported SHmax direction from the public data.

Matrix Characterization

Upper Bakken Shale structure grid was created using 173 vertical wells with log tops and limited horizontal well tops for selected control wells. The fourteen stratigraphic isopach grids were created using the same set and subset of vertical wells. The UBS structure and the five Middle Bakken stratigraphic sub-interval isochore grids used in the geomodel framework construction are shown in Figure 2. Facies (core geo-facies and log litho-facies) were not distributed in this geomodel since the 5 major sub-intervals (A through E) constrain the rock fabric types (B= packstone /sandstone, C= laminated, D= bioturbated) shown in Figure 3. The matrix porosity and matrix permeability are constrained separately to each of the 5 individual sub-intervals.

Three sets of matrix porosity were setup using NMR log porosity as input data in the geomodel. Case P1 = the NMR total porosity (TCMR) which has the best correlation with the reported core porosity. Note that the core permeability and better rock quality tends to correlate better with the NMR T2 three millisecond cutoff porosity (3MS), so a low side porosity Case P3 was setup using a NMR three millisecond porosity cutoff. An additional Case P2 that weighted averages the TCMR and 3MS porosity cases was used as the porosity base case. The weighting for this P2 case porosity is biased so that if the TCMR and 3MS porosity is similar then use almost the TCMR porosity, but if the TCMR porosity is much greater than a small 3MS porosity then use closer to the lower 3MS porosity. The three NMR matrix porosity logs used for the geomodel porosity cases P1, P2, P3 are shown in Figure 3.

Three matrix permeability data sets were setup using core analysis permeability or estimated NMR permeability. Case K1 used regression equations created from core analysis air perm data for each sub-zone. Case K2 uses the same core analysis data but as a porosity vs permeability crossplot data set to honor the data scatter when used as a cloud transform by sub-zone in the geomodel. Case K3 used the NMR estimated permeability from the KSDR log curve as hard data input to the geomodel. No net-to-gross (NTG) porosity cutoff was used in the geomodel since using a bulk volume water (BVW = 0.01) approach to estimate irreducible water saturation S_{wi} for each porosity cell

results in an effective porosity cutoff of 1.25% porosity (80% S_{wi} and 20 % S_{or}) The three matrix permeability cases used for the geomodel porosity K1 and K2 from core, and K3 from NMR KSDR are also shown in Figure 3.

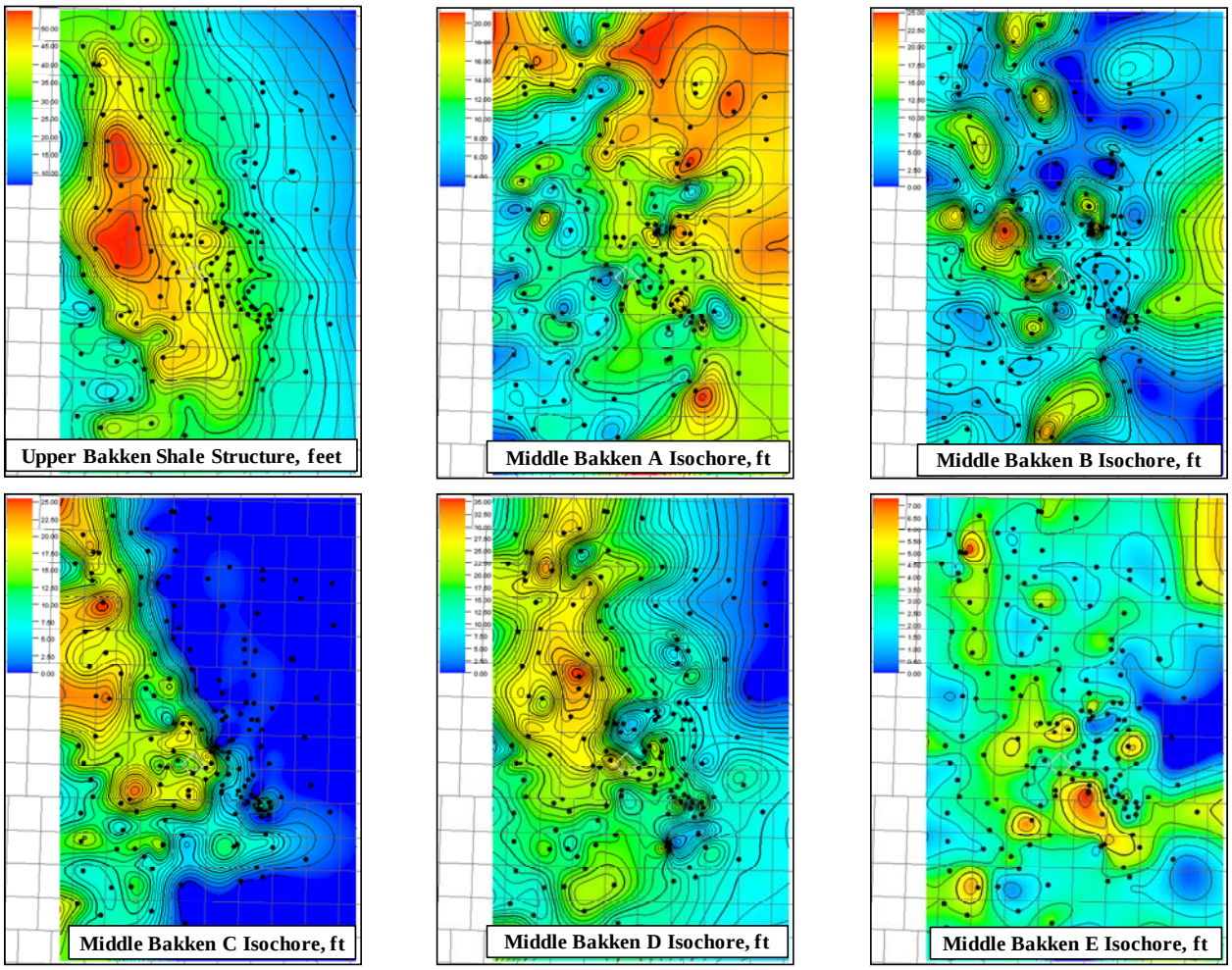

Figure 2. Upper Bakken Shale structural grid which is the controling structure grid in the geomodel. The five sequence statigraphic isochore grids (A,B,C,D,E) are shown for the Middle Bakken and are used to constrain the geomodel framework.

The Middle Bakken in the large geomodel produces a range of dry oil in updip edge areas to 50% water cut in some downdip areas. This Middle Bakken flow-simulation model area has a formation water cut that ranges from 10 to 20%. Using the apparent irreducible S_{wi} from oil base mud cores in areas that produce dry oil, the irreducible S_{wi} was set in the geomodel using a bulk volume water (BVW) relation of 0.01 (S_{wi} = BVW/porosity). Then, using the same OBM core data, we set the total SWT to be S_{wi} from BVW and added 15% mobile water (S_{wm}) to account for the higher total S_w seen in the OBM core in the model area that produces a 10 to 20 % free water cut. This increased SWT above S_{wi} was used to set the total water saturation in the simulation model.

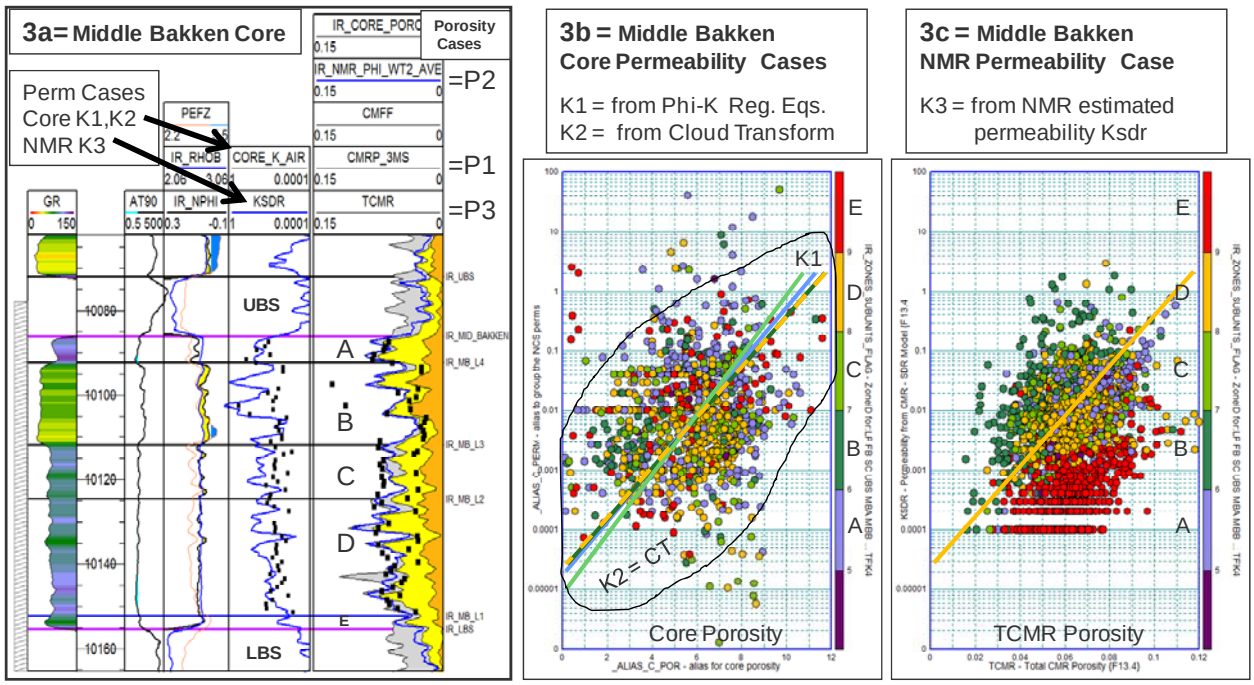

Figure 3. a) Middle Bakken subzones (A,B,C,D,E) and NMR porosity logs (cases P1,P2, P3) and NMR permeability used in case K3; b) Core porosity vs. core perm Xplot using NDIC core data from the Middle Bakken in the geomodel area. Two permeability cases are marked on this Xplot, case K1 uses core PhiK regression equations for intervals A to E, case K2 uses the same core PhiK data but as a cloud-transform in the geomodel to attempt to preserve the decade of permeability data scatter; c) NMR log permeability data used in case K3.

Fracture Characterization

The Bakken and Three Forks producing intervals are naturally fractured, some areas more than others. Ideally we would like to use a seismically conditioned data set to correlate with natural fracture indicators and develop a 3D proxy for fracture intensity and variability (Michelena, et. al. 2014); however, we have no publicly available 3D seismic data set in this area. Therefore for this paper, three cases of areal distributed possible natural fracture intensity were created for the simulation area. The first case (NF2) assumes a uniform natural fracture constant background across the entire area and is approximately equal to 20 ft between open productive fractures. The second case (NF5) used a published (NDIC GI-80 report, Anderson 2009) lineament intensity map (cumulative lineament length / sq mile) as a proxy for length of fractures per unit area (P21, 1/L). P21 was rescaled to an approximate area of fractures per unit volume (P32, 1/L) fracture intensity range and then tuned to be approximately correct for fracture permeability and fracture porosity range. Both cases NF2 and NF5 have uniform non-isotropic directions for the fracture permeability (k_{fx} and k_{fy}). The local X which is the northeast direction for flow-simulation "I" direction and is 5 times the local Y which is the northwest direction for flow-simulation "J" direction.

The third case (NF8) has non-isotropic fracture permeability. Case NF8 uses the published lineament sets from the NDIC GI-80 report and separates the published lineaments into four azimuthal fracture sets. Lineament set-1 = NE azimuth, set-2 = NW azimuth, set-3 = primarily North South and set-4 = primarily East West. For each lineament set a, distance to lineament was estimated for each grid cell. This distance to lineament parameter per grid cell was used with a power law function of fracture spacing (L) from the lineament that was dependent on distance to lineament. The set-1 lineaments (aligned with SHmax) were assigned a higher fracture density over a longer distance to lineament. The set-2 lineaments (perpendicular to SHmax) were assigned a lower fracture density over a shorter distance to lineament. All four sets were used as a continuous fracture model approximation to P32 and then analytically converted to fracture properties needed for the dual-porosity flow-simulation (shape factor σ, k_{fx}, k_{fy}, and fracture porosity).

None of these 3 cases tested vertical variation of fracture intensity based on stratigraphic sub-zones or vertical mechanical bedding, both of which could be important. Cases NF5 and NF8 are examples of CFMs. No DFN

modeling work was done for this geomodel, although limited pre-interpreted public image log data does exist in the larger geomodel area. A small initial water saturation was used in the open fractures and set at 1% S_{wi} since rugose open fracture surfaces do have some capillary bound water.

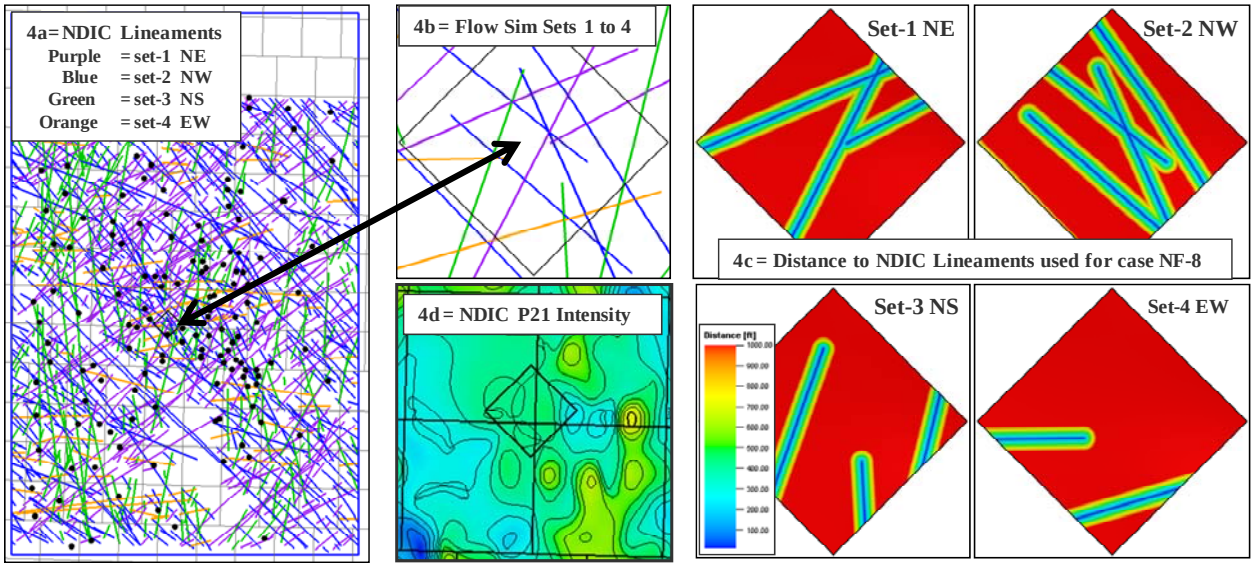

Figure 4. Two of the natural fracture distribution cases used in the geomodel and flow-simulation. a) NDIC lineaments from report GI-80 seperated into four azimuthal groups. b) Zoom-in of the same lineaments in the 9-section flow-simulation area. c) Distance-to-lineament estimate that was used to estimate decreasing fracture intensity away from the lineaments. This was done seperately for all four azimuthal groups and used in case NF8. d) NDIC lineaments from report GI-80 as a fractue intensity grid shown as total linear feet of lineaments per square mile (units are 1/L or 1/ft). This is a P21 fracture intensity map pxroxy and was rescaled for use in natural fracture case NF5.

Geomodel Construction

The initial regional area (120 township) static geomodel covers the vertical interval from the lower Lodgepole to the top of the Birdbear and includes Bakken and Three Forks productive intervals. This 427 million cell geomodel provides the flexibility to extract different Bakken and Three Forks area subsets with different vertical interval combinations for the GPU flow-simulator testing of what-if cases.

The geomodel area grid is aligned North-South and the area cell size is 250 ft x 250 ft and later reduced locally to 40 ft x 40 ft to allow for capturing finer details for the later flow-simulation model. The geomodel structural framework was constructed using one master structure surface for the Upper Bakken Shale and subtracting 2 isochores above the UBS structure for the Scallion, False Bakken and a 80 ft slice of the lower Lodgepole to create the major stratigraphic zones above the UBS. Then, we added 12 isochores below the UBS structure: 1 for the UBS, 5 Middle Bakken sub-intervals, 1 LBS, and 5 major sub-interval isochores for the Three Forks. Proportional layering was used for the internal fine vertical layering (approximate 2-ft layers) inside each of the 14 stratigraphic sub-intervals.

No geo-facies or litho-facies were distributed in this model, since the 5 Middle Bakken sub-intervals basically constrain the major geo-facies types (B= packstone/sandstone, C= laminated, D= bioturbated) All three NMR log matrix porosity cases (P1= TCMR, P2= weighted average of TCMR+3MS, and P3= 3MS) were distributed using one sequential Gaussian simulation (SGS) geostatistic realization using a long range isotropic variogram. No porosity cutoff was used for net-to-gross (NTG) in the geomodel. Figure 5 shows an example of the porosity distribution in the geomodel.

The three matrix permeability cases were locked to the prior matrix porosity distribution. Matrix permeability case K1 used core Phi-K cross-plot regression equations for each Middle Bakken sub-interval. Matrix permeability case K2 used a geostatistical cloud-transform algorithm to approximately distribute in the geomodel the core data scatter observed in the core porosity versus permeability data for each Middle Bakken sub-interval. Matrix permeability

case K3 used the NMR permeability estimated from logs (KSDR) and distributed in the model using the same SGS geostatistic algorithm as was used for the porosity distributions.

Irreducible water saturation was first distributed using bulk volume water (BVW = .01) to estimate irreducible water saturation (S_{wi}) based on nearby dry oil production areas that had OBM core data. Since this flow-sim model area does produce a 10 to 20% free water cut in the Middle Bakken, the water saturation in the 9 section flow-simulation area was approximated by setting the average water saturation (SWT) to be S_{wi} from BVW and then adding 15% mobile water (S_{wm}). This higher SWT creates a mobile water saturation similar to the increased SWT seen in downdip OBM core data where the wells do produce a free water cut.

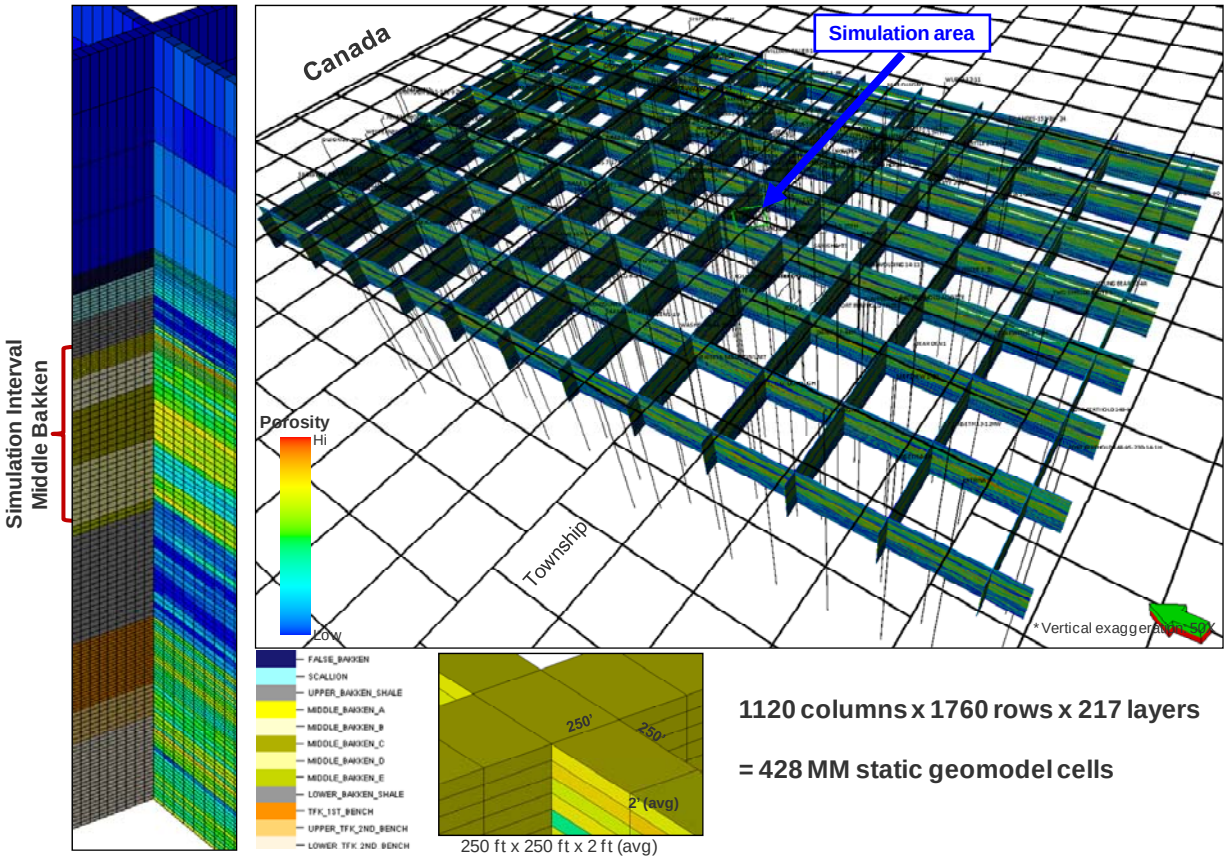

Figure 5. Fence diagram view of the Middle Bakken porosity for the 120 township geomodel. The inset shows the fine layer gridding used in the large area geomodel. Note that for the smaller flow-simulation model area, cells were downscaled to 40 ft x 40 ft and the vertical layers were upscaled from the 2 ft geomodel layering.

For this GPU flow-simulation test, a quarter township (9 square mile) subset with 5.6 million matrix cells for just the Middle Bakken was extracted from the original large geomodel in the Sanish Field area and upscaled to both a Middle Bakken 10 layer (case L2) and 20 layer (case L3) flow-unit model.

The original geomodel 250 ft x 250 ft cell size was downscaled to 40 ft x 40 ft for the flow-simulation in order to better define SRV regions and to track pressure fronts. Also the flow-simulation areal grids I-J axes were rotated from North-South so that the I-direction is aligned along the average N45E maximum horizontal stress direction (SHmax). This N45E I-direction is a local approximation of the public stress data which ranges from N30E to N60E in the larger geomodel area. This allows one of the grid axis directions (I) to be aligned along the HF stage propagation direction helping capture the major natural fracture lineaments, and aligns the SRV with SHmax.

The thirty-six 2-ft fine layers (5.6 million matrix cells before upscaling) were used in the Middle Bakken geomodel and were vertically upscaled for the flow-simulation nine-section model using approximate flow units within each of the five geologic sub-intervals. Figure 6 shows the base case of 10 flow units (case= L2) and the additional

preserved detail using 20 flow units (case L3) in the same Middle Bakken flow-simulation vertical interval. The flow-simulation model is dual porosity, so the upscaled matrix cell totals are doubled for the actual flow-simulation. The 10 flow unit case (L2) has 1.56 million matrix cells and with the additional fracture cells the total model has 3.12 million active flow-simulation cells. The 20 flow unit case (L3) has 3.12 million matrix cells (6.24 million active flow-simulation cells). Table 1 summarizes the larger geomodel cases and smaller flow-simulation cases.

Table 1. Summary of geomodel and flow-simulation model grid dimensions

Model	Stratigraphic Intervals	NI	NJ	NK	DI	DJ	DK	Orientation	Number active cells
Geomodel	10	1120	1760	209	250	250	2 (avg.)	NS	412 MM
Geomodel with subintervals	15	1120	1760	218	250	250	2 (avg.)	NS	428 MM
Simulation Grid (L2)	5	395	395	10	40	40	8 (avg.)	N45E	1.56 MM
Simulation Grid (L3)	5	395	395	20	40	40	4 (avg.)	N45E	3.12 MM
Simulation Grid (L4)	5	395	395	36	40	40	2 (avg.)	N45E	5.62 MM

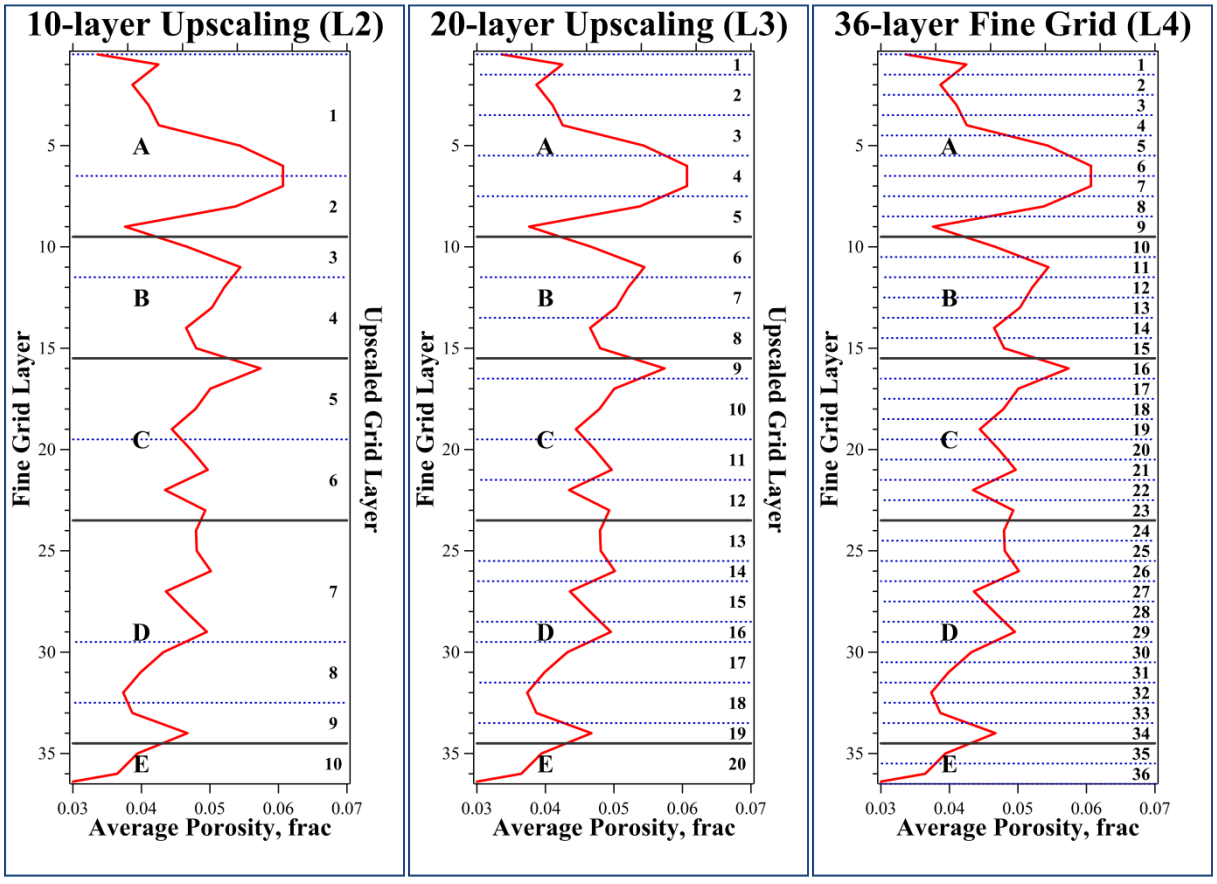

Figure 6. Three of the vertical upscale cases used for the flow-simulation model. Case L2 is a 10-layer flow-unit model upscaled from 2-ft layering to approximately a 8-ft average layer. Case L3 is a 20 layer flow-unit model upscaled from 2-ft layering to approximately a 4-ft average layer. Case L4 has no upscaling and retains all 2-ft vertical layering.

Flow-Simulation Using a GPU-based Simulator

Analytical models for reservoir modeling are fast and easy to setup, but they tend to be limited to one well at a time and are not good at predicting well infill, well interference effects, or changes in well performance due to multi-phase effects especially in dual-porosity media (Mukundakrishnan et. al., 2015). DFN models can be useful in resolving the fractures in greater detail and modeling flows within such fractures but their use is limited to small scale systems and scaling to larger areas require significant upscaling. Numerical flow-simulation models based on dual-medium models fall in between the analytical and DFN techniques in terms of model complexity description. Such models can capture sufficient details of fluid flow physics, geology and well completions (Fig. 7a). However, such numerical models that run on CPU-based simulators tend to be computationally expensive when simulating large models with tens of millions of cells. GPUs offer a promising alternative to drastically reduce the run times and also simulate very large models (Esler et. al. 2014, Mukundakrishnan et. al., 2015).

Since about 2007, GPUs have been used increasingly in the oil and gas industry to accelerate computationally demanding workflows, primarily in seismic processing (Weiss and Shragge, 2013). Making effective use of their raw performance for reservoir simulation requires redesigning key solver algorithms and reengineering the code base to expose an abundance (tens of thousands) of independent tasks that can be executed in parallel. This is due to the very large number of independent computational cores present in a GPU compared to the CPU (Fig. 7c). The GPU flow simulator (echelon) used in this work (Esler et. al., 2015) can handle 10 to 50 million cells dual-porosity unconventional models with runtimes in the 6 to 60 minute runtime range for 20 to 30 year forecasts using a single node of 8 Tesla K40 GPUs (Fig. 7b). The results are in excellent agreement with those from a commercial CPU-based simulator, with typical discrepancies less than 0.01%. It should be noted that the GPU simulator used in this work has not yet implemented all the complexities involved in reservoir modeling. For the given set of implemented features (complexities) in this study, the performance of GPUs is much faster than other available CPU-based solutions and can also accommodate larger model sizes.

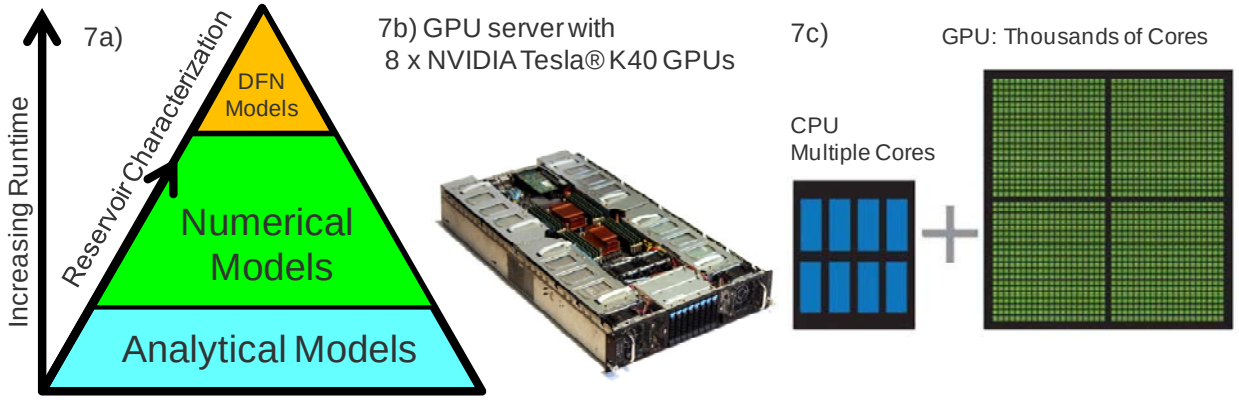

Figure 7. a) A conceptual diagram showing how numerical flow-simulation models compare to analytical and DFN models. The fast GPU-based numerical models allow additional reservoir charaterization detail to be retained compared to CPU-based numerical models for the same model runtimes; b) NVIDIA GPU processor used in this paper; c) Conceptual sketch showing the relative increase in processing cores that are partially responsible for the reduced run time when using GPU numerical flow-simulation.

Bakken Flow-simulation Case Description

To keep the different flow-simulation cases organized, each major geomodel variable was assigned a short identifer for that case and the individual case variables were combined into a flow-simulation "case name" that captures the choices used in that flow-simulation run. Table 2 below summarizes the subsets of name identifiers for upscale layering, matrix perm and porosity input cases and different natural fracture cases. For example, the 10 flow unit base case name was W1_H1_L2_P2_K3_S1_N1_NF2_VF which is used to identify which well pattern (W1) and hydro-frac SRV (H1_VF) were combined with an upscaling choice (L2) and which geomodel matrix variables (P2, K3, S1, N1) and which natural fracture case (NF2) were used for that specific flow-simulation case.

Table 2. Input case descriptions

Variable Type	Name	Variable Name Description
Area Well Paths	W1	B zone: Test one well per section, minimal well interference
Area Well Paths	W2	B zone: Test multi wells per section spacing and lengths
Hydro-Frac SRV	H1_Uf	Fixed hydrofrac length with uniform SRV properties
Hydro-Frac SRV	H1_Vf	Fixed hydrofrac length with non- uniform SRV properties
Upscale Layers	L2	10 matrix flow units
Upscale Layers	L3	20 matrix flow units
Matrix Porosity	P1	Max case= Porosity from NMR total porosity TCMR
Matrix Porosity	P2	Base case= Porosity from Wt. Ave. of TCMR and 3MS
Matrix Porosity	P3	Min case= Porosity from NMR 3MS porosity
Matrix Perm	K1	Core Air Perm from PhiK Regression Eq. by zone
Matrix Perm	K2	Core Air Perm from PhiK Cloud Transform by zone
Matrix Perm	K3	NMR perm estimated from KSDR method
Water Saturation	S1	S_{wi} from BVW = 0.01 and add mobile water S_{wm} = 15%
Net-2-Gross NTG	N1	No NTG cutoffs used but BVW=0.01 effectively 1.25% cutoff
Natural Fractures	NF2	Uniform natural fracture spacing of 20 ft
Natural Fractures	NF5	Non-uniform fracture intensity from re-scaled GI-80 P21 map
Natural Fractures	NF8	Non-uniform fracture intensity from GI-80 lineaments (4 sets)

All flow-simulation models were initialized using PVT data that was adjusted to the local area model GOR using the geomodel well Nelson Farms 1-24H located 12 miles North of the flow-simulation area. The original PVT data was from the NDIC well file (API 33061004890000) that included a Pencor PVT report and was checked against other reported Bakken PVT data (Du. et. al., 2012). The initial reservoir pressure was 6,965 psia at bottom-hole temperature of 245 deg F and was taken from nearby NDIC well file reports and adjusted for the average TVDss depth of the flow-simulation model. The minimum producing bottom-hole pressure (BHP) for the flow-simulation model was set at 750 psia.

Matrix and fracture rock compaction data were taken from public data (Chu, et. al. 2012) and adjusted based on our Bakken experience. Relative permeability curves for oil, water and gas were taken from public data (Perapon, et. al. 2014) and adjusted to fit locally produced water cuts. End-point scaling was used with the relative perm curves so that poor matrix has higher irreducible S_{wi} and good matrix has lower S_{wi}. No capillary pressure curves were used for these flow-simulation runs. Table 3 summarizes the average flow-simulation matrix and fracture properties prior to any flow-simulation tuning of the fracture properties.

Table 3. Summary of the fracture and matrix static properteis used in the flow-simulation, prior to any tuning of the fractue properties

Parameter	Min. Value	Max. Value	Ave. Value
P1: TCMR Porosity, frac	0.016	0.145	0.064
P2: TCMR+CMRP_3MS Combined Porosity, frac	0.013	0.117	0.058
P3: CMRP_3MS Porosity, frac	0.009	0.092	0.049
K1: Regression Equation Permeability, mD	0.0003	2.000	0.0679
K2: Cloud Transform Permeability, mD	0.0001	2.000	0.0421
K3: KSDR Permeability, mD	0.0000	1.0627	0.0118
NF5: Sigma Factor, $1/ft^2$	0.00277	0.01072	0.00864
NF5: Fracture Porosity, frac	0.0000863	0.000170	0.000152
NF5: Fracture Permeability X, mD	0.0390	0.0768	0.0687
NF5: Fracture Permeability Y, mD	0.0390	0.0768	0.0687
NF8: Sigma Factor, $1/ft^2$	0.0064	2.0061	0.0196
NF8: Fracture Porosity, frac	0.000276	0.00378	0.000323
NF8: Fracture Permeability X, mD	0.217	3.684	0.258
NF8: Fracture Permeability Y, mD	0.145	2.892	0.164

The multi-stage hydraulic fractures (HF) were spaced approximately every 320 ft. The HF and SRV were defined by two separate cases: one as uniform (UF) properties and one as non-uniform (VF) properties. The properties approximate the average of the historical work in this area. For the uniform case, the HF half-length is 220 ft and conductivity ($k_f w_f$) is 100 md-ft. The non-uniform case used the same HF half-length of 220 ft, however the fracture conductivity has a tapered reduction with length and height resulting in average conductivity of 80 md-ft. For the uniform case, the SRV half-length is 420 ft, with a SRV half-width of 140 ft. Permeability of the SRV region (k_{srv}) is 0.5 md for the uniform case. The non-uniform SRV has about the same average permeability (0.5 md) but tapers to a minimum value 0.25 md at the edge of the SRV area. The non-uniform HF and SRV are illustrated in Figure 8 showing the modeled linear decline in the HF properties and exponential decline in SRV properties in each of the three directions.

Simulation Case Results

As described by the previous geologic model realizations, we ran a number of different simulations to test the impact of model parameters on forecast results. We ran forecasts for a 24-year period, limiting time-steps to no more than 31 days. All wells start at the same time at a fixed BHP of 750 psia with a 1000 BPD maximum oil rate. Model sizes were either 3.1 or 6.2 million cells for the nine-section simulation area as described earlier. The models had either 9 or 21 wells with hydraulic fractures every 320 ft. The 9-well case has nine one-mile wells centered in each section. This case was used to check geologic and engineering sensitivity without offset well interference effects. A 21-well development case tested a variety of well lengths (Figure 8), and is equivalent to approximately 36 miles of total well length with nearly 600 fracture stages. One well in the upper left corner (Figure 8) was left in an undeveloped section with no offset to illustrate the impact of well spacing. Hydraulic fracture and SRV size and properties were defined by a programmatic workflow that sets, length, width and variable conductivity from well to SRV boundaries using the properties described earlier. Hydraulic fracture height was equal to total middle Bakken thickness. Properties were defined to roughly honor estimated total production for the public information available in the AOI.

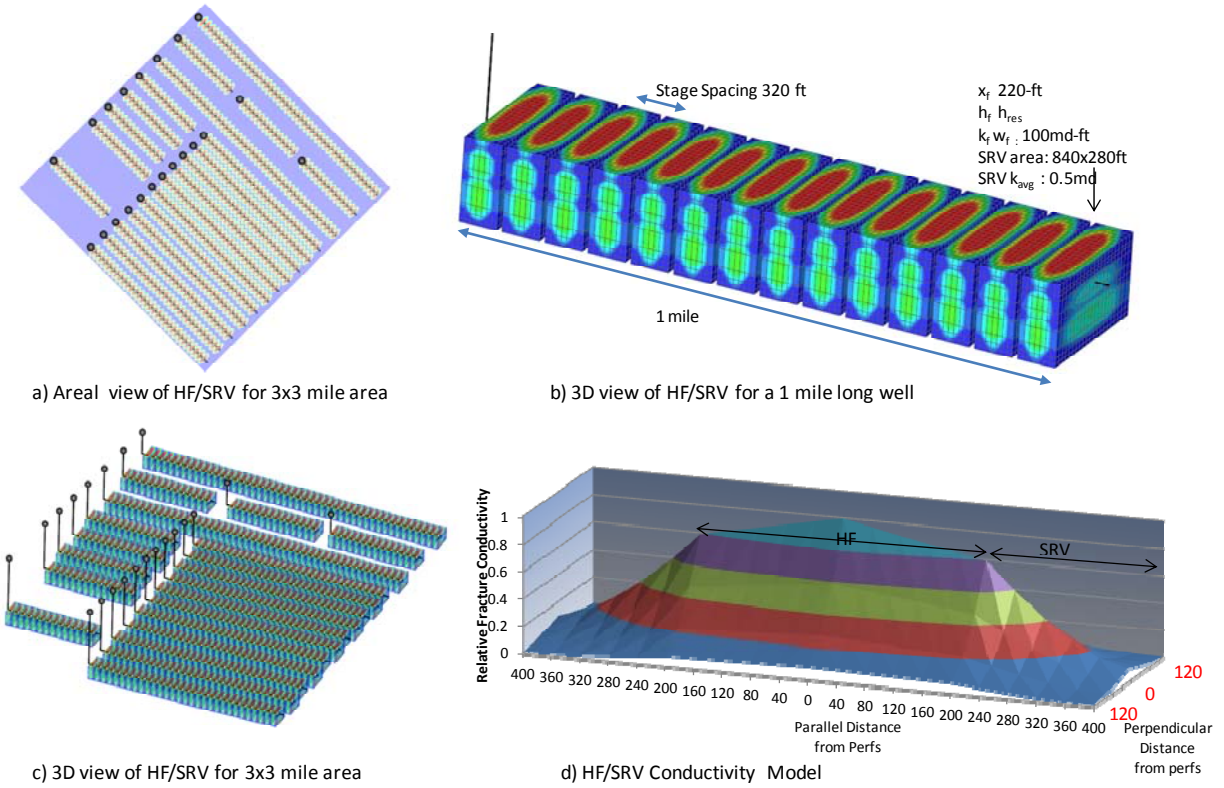

Figure 8. Illustration of SRV and hydraulic fracture realizations used in this paper. HF are spaced every 320 ft. HF/SRV conductivities varies along the height, length and width; a) Areal view of the HF/SRV area along the wells, b) SRV areas which nearly overlap along the well length, c)3D view for all wells and d) HF/SRV conductivity variation with distance (height variation not shown).

The simulations were ran on NVIDIA Tesla® K40 or K80 GPU cards (accessing 3-4 GPUs per simulation run). Access to two 8-GPU racks allowed simultaneous throughput of 4 runs. Model run times vary from as low as 5 minutes to over 40 minutes depending on size of problem, number of GPUs, GPU card type and non-linearity resulting in reduced time steps. Based on a limited number of comparison runs, we expect CPU run time to be 5-20 hours, again depending on size, number of parallel processors and model stability. The 40 runs presented here represent less than 8 hours of GPU clock time, showing that thousands of realization are practical in a reasonable time-frame.

Figures 9 through 11 compare simulation results for a number of different realizations. Each figure shows the run for one particular set of natural fractures (NF2, NF5 and NF8). The differences in OOIP are a result of using either the P1, P2 or P3 matrix porosity realizations. The grouping of higher total oil production represents the W2 well cases (21 wells) while the lower set are the 9-well W1 cases. Similar separation is shown for the water-cut and gas-oil ratio. There is additional small scale variation within each of these larger sets as a result of different matrix permeability sets and simulation layering. The most noticeable outliers in the total oil production for the 21-well case are for higher (P1) or lower (P3) matrix porosity. The limited impact for matrix permeability and stratigraphic detail (model layering) in these cases is a result of the high fracture intensity in this area of the Bakken. Figure 12 compares the NF2, NF5 and NF8 simulations for the P2-K3 realization and the nine-well model. These results show the important impact of the fracture description with the higher recovery coming from the more complex NF8 case and the lowest recovery from the uniform NF2 case. For each realization, the 20-layer model gives slightly lower recovery than the 10-layer model.

Several model properties and the well configuration for the 21-well case are illustrated in Figure 13. The vertical exaggeration is 10x. Figure 14 shows pressure distribution after 1-year of depletion. The main natural fracture lineaments are drawn as polylines. Recall that all wells start at the same time. The well in the upper left corner (one well in one section) clearly shows limited areal depletion while the closely spaced wells show full interference throughout the area. This is a function of the fracture and matrix properties illustrating the importance of geologic characterization. In these cases natural fracturing leads to efficient depletion of the matrix; in other areas of the Bakken with less natural fracturing, we would see more impact of the matrix permeability and stratigraphic variability. Table 4 summaries 40 simulations showing in-place values, 24-year recovery and simulation time. The green highlighting denotes the changes for each run using the acronyms noted in Table 2.

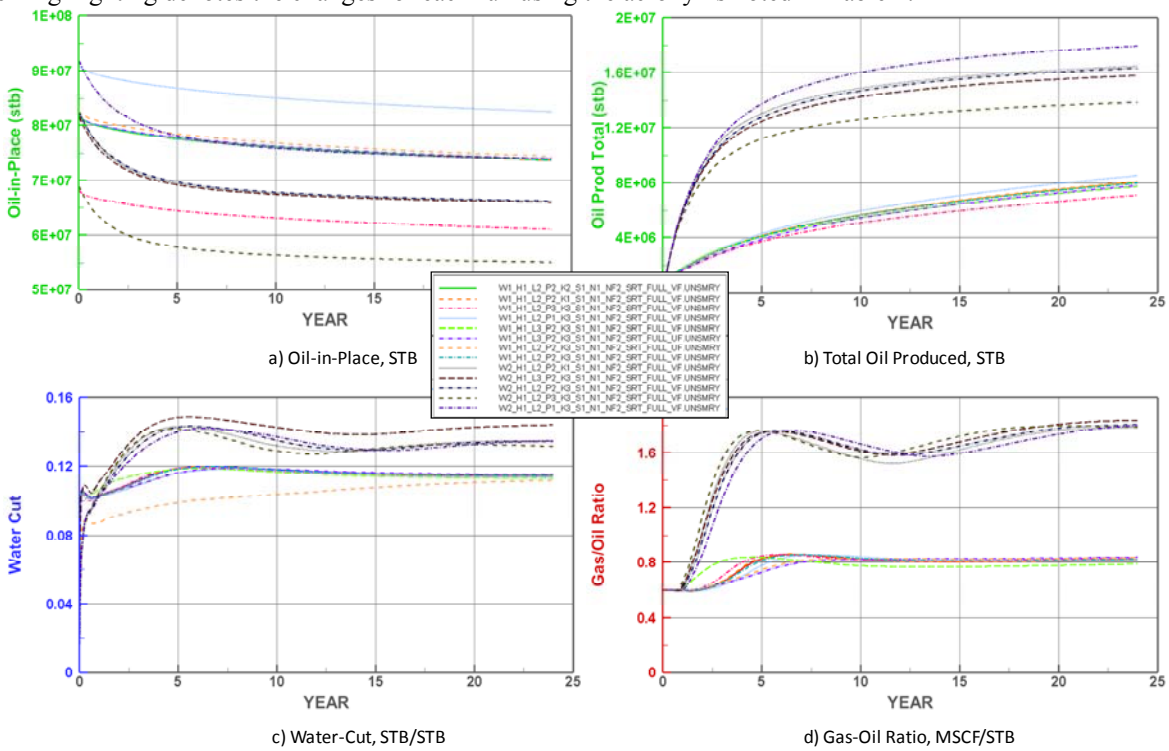

Figure 9. a) Oil-in-place, b) Total Oil Produced, c) Water-cut and d) Gas-Oil Ratio for uniform natural fracture set 2 (NF2). The grouping of higher total oil production represents the W2 well cases (21 wells) while the lower set are the 9-well W1 cases.

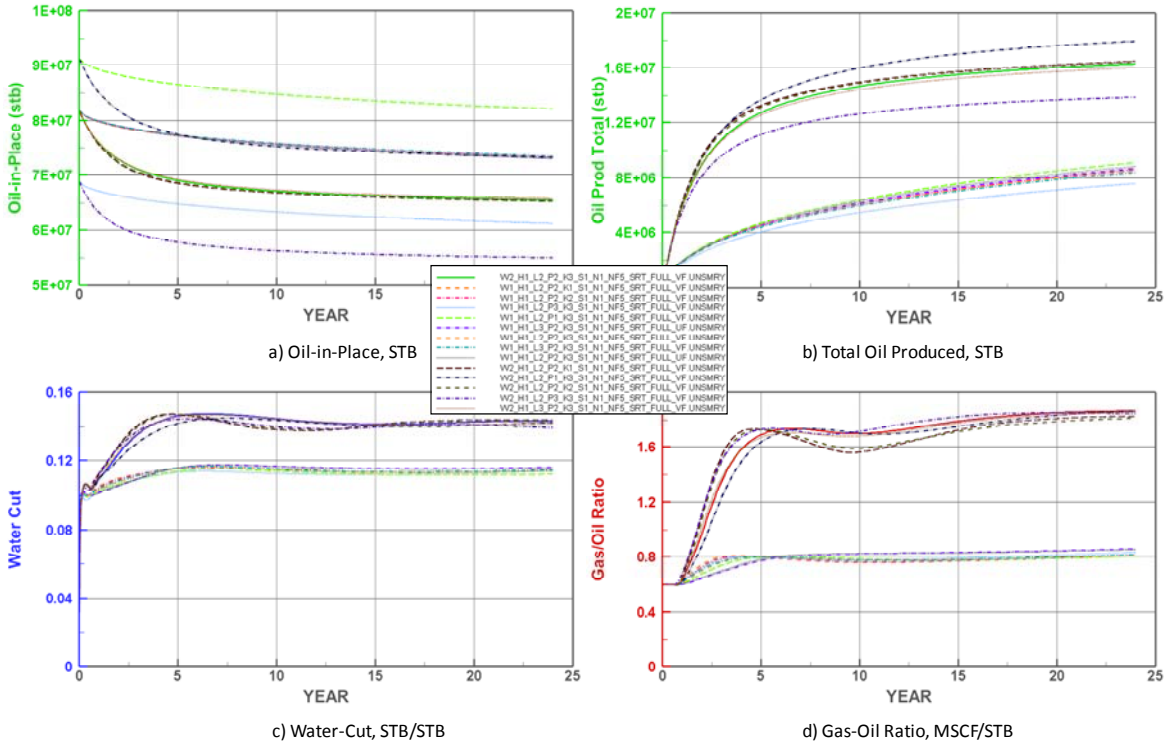

Figure 10. a) Oil-in-place, b) Total Oil Produced, c) Water-cut and d) Gas-Oil Ratio for complex natural fracture set 5 (NF5). The grouping of higher total oil production represents the W2 well cases (21 wells) while the lower set are the 9-well W1 cases.

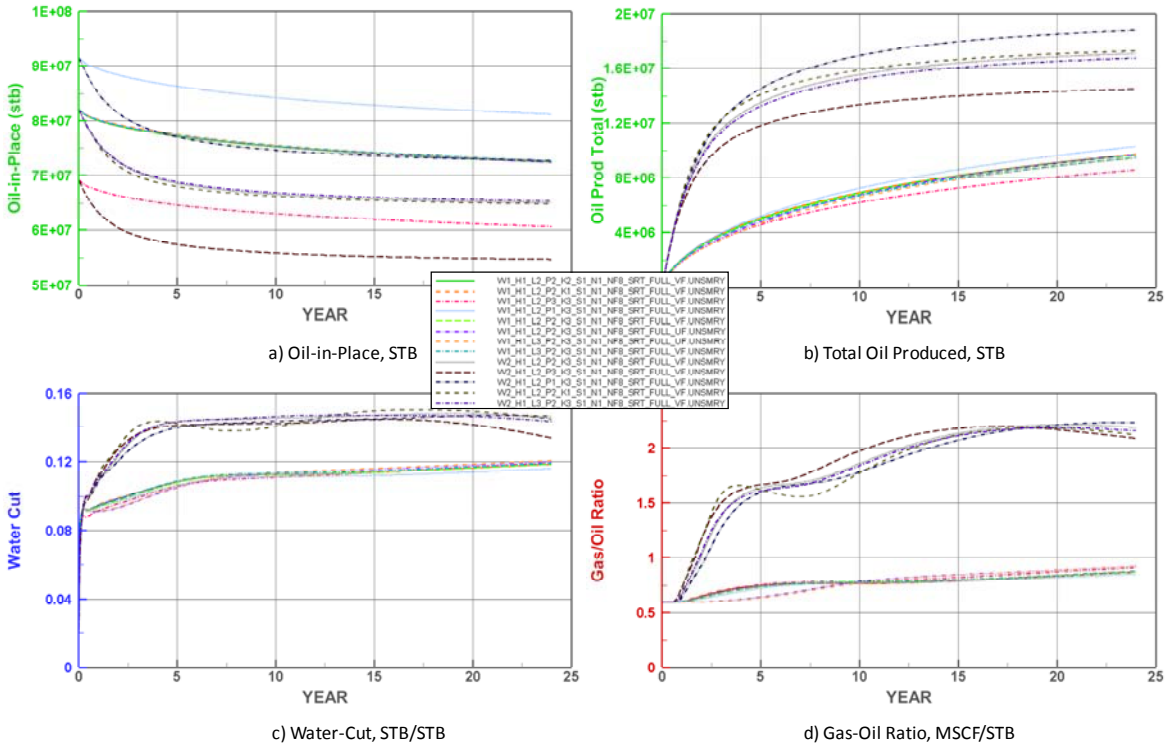

Figure 11. a) Oil-in-place, b) Total Oil Produced, c) Water-cut and d) Gas-Oil Ratio for complex natural fracture set 8 (NF8). The grouping of higher total oil production represents the W2 well cases (21 wells) while the lower set are the 9-well W1 cases.

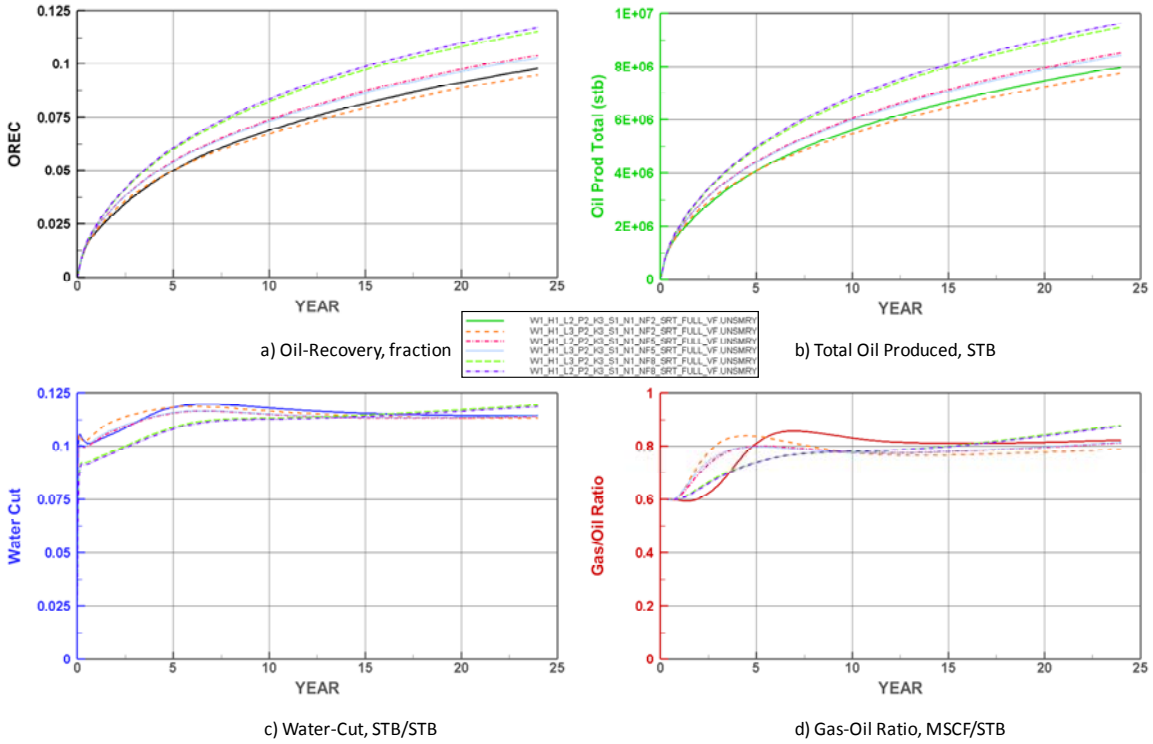

Figure 12. a) Oil Recovery, b) Total Oil Produced, c) Water-cut and d) Gas-Oil Ratio comparing natural fracture sets NF2, NF5 and NF8 for the nine-well case and 10 or 20 simulation layers. The highest recovery comes from the more complex NF8 case and the lowest recovery from the uniform NF2 case. Recoveries estimated from 10- and 20-layer models are similar.

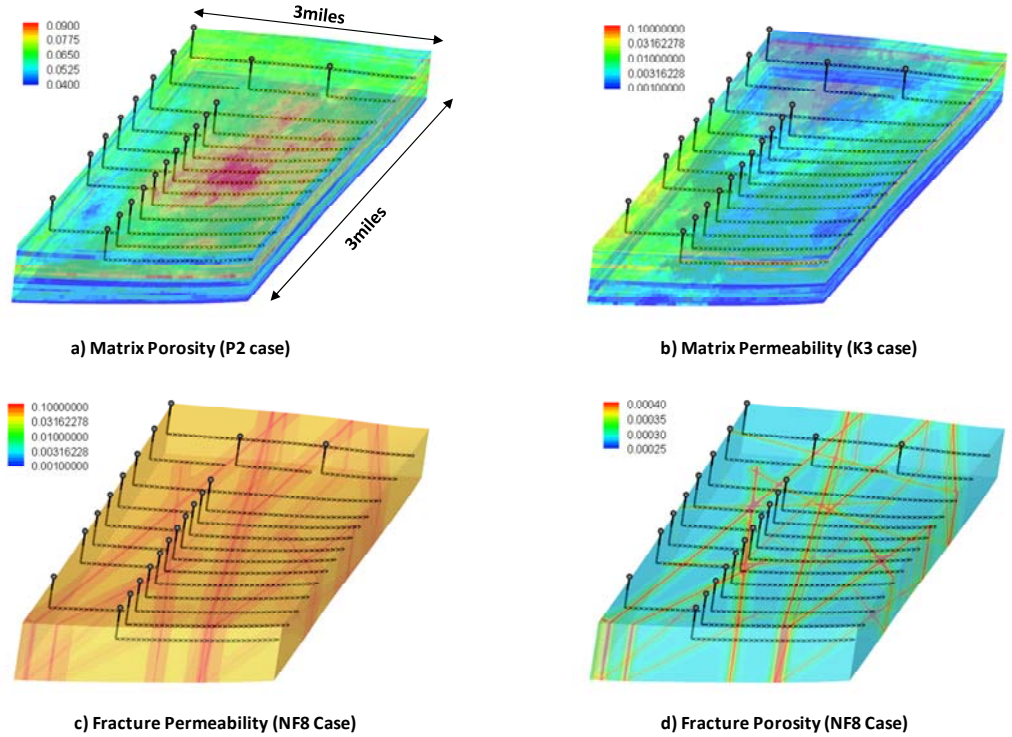

Figure 13. Matrix and fracture porosity and permeability for the model cases noted.

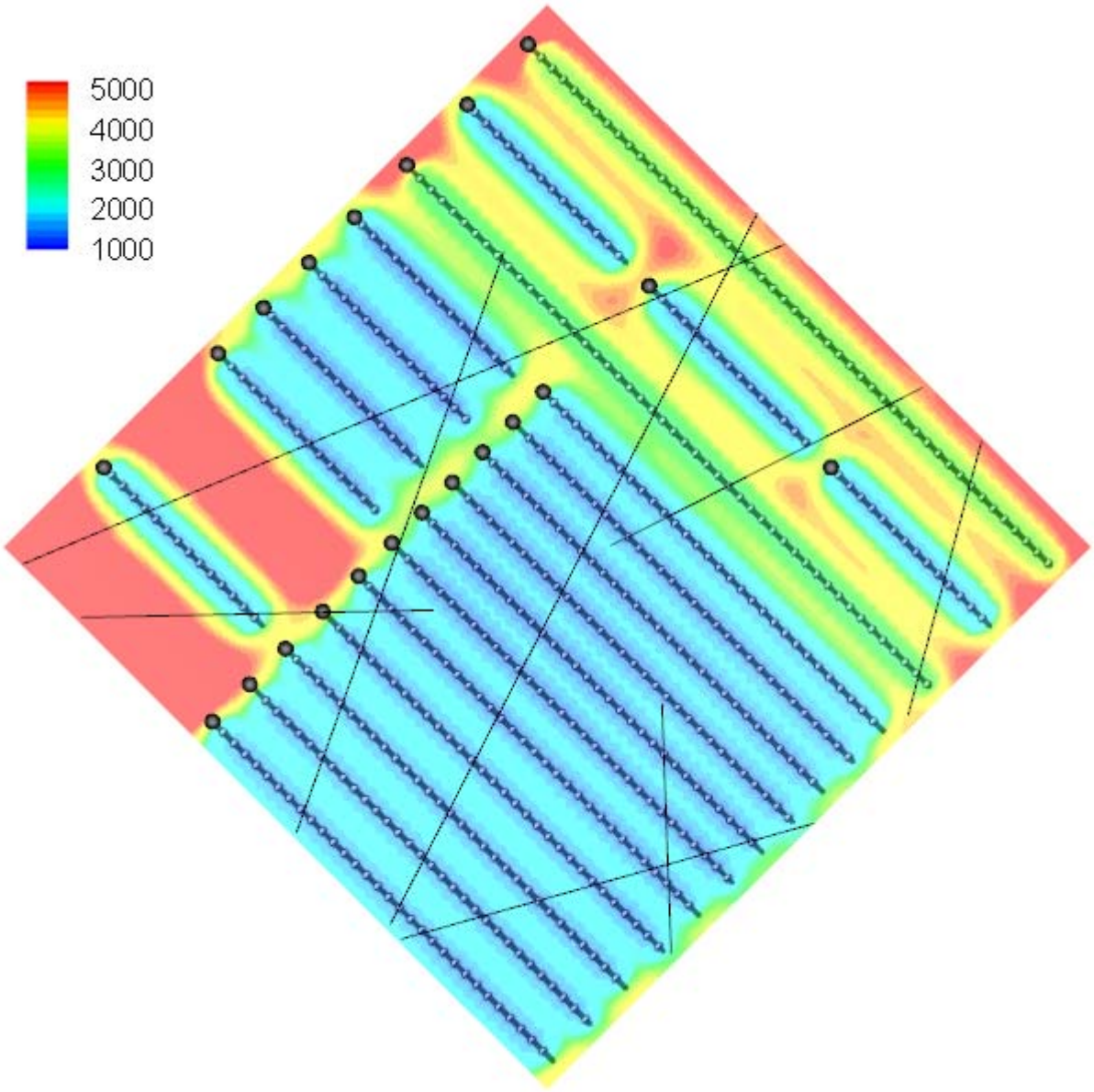

Figure 14. Fracture pressure (average over all layers after one-year of depletion) for the 21-well model, fracture realization NF8. The fracture lineaments are noted. The well in the upper left corner (1 well in one section) clearly shows limited areal depletion while the closely spaced wells show full interference throughout the area. This is a function of the fracture and matrix properties illustrating the importance of geologic characterization.

Table 4. Simulation run summary showing in-place values, 24-year recoveries and simulation time. Total time for these runs is less than 8-hours. The green highlighting denotes the changes for each run using the acronyms noted in Table 2. Shading shows the grouping by fracture characterization set (NF2, NF5 and NF8).

NFR CASE	WELL CASE	LAY. CASE	PHIM CASE	KM CASE	HF CASE	NP, MMSTB	WP, MMSTB	GP, MMSTB	PAV psia	OOIP, MMSTB	OWIP, MMSTB	OGIP, BSCF	Rec, % OOIP	GPU Min
NF2	W1	L2	P2	K1	VF	8.04	1.01	5.86	2338	81.69	51.17	49.01	9.84%	15.1
NF2	W1	L2	P2	K2	VF	8.03	1.01	5.85	2338	81.69	51.17	49.01	9.83%	6.7
NF2	W1	L2	P1	K3	VF	8.53	1.06	6.19	2514	91.07	56.06	54.64	9.37%	5.9
NF2	W1	L2	P2	K3	UF	8.11	0.88	5.87	2372	81.69	51.18	49.51	9.93%	4.9
NF2	W1	L2	P2	K3	VF	7.98	1.00	5.82	2367	81.69	51.17	49.01	9.77%	6.7
NF2	W1	L2	P3	K3	VF	7.11	0.89	5.23	2143	68.17	42.75	40.90	10.43%	5.5
NF2	W1	L3	P2	K3	UF	7.81	0.98	5.63	2449	81.69	51.16	49.02	9.56%	9.1
NF2	W1	L3	P2	K3	VF	7.75	0.98	5.70	2473	81.69	51.16	49.02	9.48%	13.5
NF2	W2	L2	P2	K1	VF	16.47	2.13	17.41	1006	81.69	51.18	49.51	20.16%	14.9
NF2	W2	L2	P1	K3	VF	17.94	2.31	18.78	1098	91.07	56.08	55.14	19.70%	9.3
NF2	W2	L2	P2	K3	VF	16.33	2.10	17.23	1058	81.69	51.18	49.51	19.99%	6.8
NF2	W2	L2	P3	K3	VF	13.87	1.75	14.77	1026	68.17	42.76	41.40	20.35%	7.5
NF2	W2	L3	P2	K3	VF	15.80	2.24	16.76	1160	81.69	51.16	49.02	19.34%	43.0
NF5	W1	L2	P2	K1	VF	8.59	1.06	6.27	2064	81.80	51.17	49.08	10.50%	7.2
NF5	W1	L2	P2	K2	VF	8.58	1.06	6.25	2065	81.80	51.17	49.08	10.49%	7.8
NF5	W1	L2	P1	K3	VF	9.10	1.11	6.59	2232	91.18	56.07	54.71	9.98%	5.9
NF5	W1	L2	P2	K3	UF	8.83	1.09	6.48	2025	81.80	51.17	49.08	10.79%	6.1
NF5	W1	L2	P2	K3	VF	8.51	1.05	6.20	2100	81.80	51.17	49.08	10.41%	6.9
NF5	W1	L2	P3	K3	VF	7.60	0.92	5.58	1926	68.87	42.34	41.32	11.04%	7.0
NF5	W1	L3	P2	K3	UF	8.68	1.08	6.35	2106	81.80	51.16	49.08	10.61%	10.3
NF5	W1	L3	P2	K3	VF	8.42	1.04	6.14	2168	81.80	51.16	49.08	10.29%	15.0
NF5	W2	L2	P2	K1	VF	16.47	2.31	17.61	965	81.80	51.17	49.08	20.14%	21.3
NF5	W2	L2	P2	K2	VF	16.44	2.31	17.51	971	81.80	51.17	49.08	20.10%	39.2
NF5	W2	L2	P1	K3	VF	17.93	2.48	18.90	1061	91.18	56.07	54.71	19.66%	10.5
NF5	W2	L2	P2	K3	VF	16.30	2.28	17.33	1023	81.80	51.17	49.08	19.92%	8.9
NF5	W2	L2	P3	K3	VF	13.87	1.91	14.90	1002	68.87	42.34	41.32	20.14%	10.9
NF5	W2	L3	P2	K3	VF	16.02	2.24	17.01	1130	81.80	51.16	49.08	19.58%	27.9
NF8	W1	L2	P2	K1	VF	9.73	1.14	6.97	1723	82.15	51.18	49.29	11.85%	8.5
NF8	W1	L2	P2	K2	VF	9.71	1.14	6.95	1724	82.15	51.18	49.29	11.82%	7.0
NF8	W1	L2	P1	K3	VF	10.29	1.19	7.29	1850	91.53	56.07	54.92	11.24%	5.8
NF8	W1	L2	P2	K3	UF	9.70	1.12	6.80	1759	82.15	51.18	49.29	11.80%	4.7
NF8	W1	L2	P2	K3	VF	9.62	1.12	6.87	1768	82.15	51.18	49.29	11.71%	5.0
NF8	W1	L2	P3	K3	VF	8.59	0.98	6.22	1685	69.23	42.35	41.54	12.41%	5.1
NF8	W1	L3	P2	K3	UF	9.47	1.10	6.61	1858	82.15	51.17	49.28	11.53%	8.8
NF8	W1	L3	P2	K3	VF	9.47	1.11	6.78	1856	82.15	51.17	49.28	11.53%	12.6
NF8	W2	L2	P2	K1	VF	17.26	2.36	18.93	879	82.15	51.18	49.29	21.02%	22.9
NF8	W2	L2	P1	K3	VF	18.81	2.54	20.31	971	91.53	56.07	54.92	20.54%	8.5
NF8	W2	L2	P2	K3	VF	17.07	2.32	18.61	941	82.15	51.18	49.29	20.78%	10.3
NF8	W2	L2	P3	K3	VF	14.50	1.93	15.95	927	69.23	42.35	41.54	20.94%	9.1
NF8	W2	L3	P2	K3	VF	16.74	2.29	18.21	1052	82.15	51.17	49.28	20.38%	25.0

Summary and Conclusions

Massively-parallel GPU simulation is applied for the first time to a realistic large Bakken geomodel. First, we developed a large 427 million cell (120 township) Bakken/Three Forks static geomodel using public domain data. Geologic data used in the geomodel construction creates alternate plausible cases for matrix and natural fracture characterization to address a wide range of Bakken geologic sensitivities and their impact on Bakken well performance. We ran flow simulations on 3.1 to 6.2 million cells models (one-quarter township, Middle Bakken) on a modern GPU simulator. Simulation results show the importance of matrix porosity estimates, natural fracture characterization and SRV description. We demonstrate how a modern GPU flow simulator provides the ability to run multiple fine-scale realizations with groups of Bakken only horizontal well sets to rapidly test well spacing and geologic uncertainty using dual-porosity flow-simulation models.

Acknowledgement

The authors would like to thank the North Dakota Geologic Survey and NDIC for the vision to retain the Bakken geology (core, logs, pressures, well-reports) and Bakken engineering monthly production data by well that made the construction of this Bakken and Three Forks geomodel possible. We would also like to thank Marathon Oil Corp. for funding the proof-of-concept GPU flow-simulation work, in particular David Brimberry, Richard Uden, Edward Yang and Don Caldwell for their support. We appreciate the use of the NVIDIA Tesla® 8xK40/K80 GPU servers to run the multi-million cell flow-simulation models. We finally would like to acknowledge Kevin Godbey at iReservoir for software coding of the HF/SRV algorithm and Teresa Schaller for assistance in setting up the hydraulic fractures in the models and for making numerous simulation runs.

Nomenclature

BVW = porosity*irreducible water saturation (ϕS_{wi})
h = height, ft
k_{fx} = fracture permeability in x-direction, mD
k_{fy} = fracture permeability in y-direction, mD
k_{srv} = SRV permeability, mD
L = fracture spacing, ft
P21= length of fractures per unit area, 1/L
P32 = area of fractures per unit volume, 1/L
q = flow rate, STB/D
S_w = water saturation, fraction
S_{wm} = mobile water saturation, fraction
S_{wi} = irreducible water saturation, fraction
SHmax = maximum horizontal stress, mPa
t = time, days
w_f = fracture width, ft
ϕ = porosity, fraction
σ = matrix shape factor, $1/L^2$

References

F. J. Anderson: "Lineament Mapping and Analysis in the Northeastern Williston Basin: Exploration and Production Trends in the Parshall Area, North Dakota" Geologic Investigations Report GI-80 by the North Dakota Geologic Survey (2009) download available at https://www.dmr.nd.gov/ndgs/bakken/bakkenthree.asp

L. Chu, P. Ye, I. Harmawan, L. Shepard, "Characterizing and Simulation the Non-stationariness and Non-linearity in Unconventional Oil Reservoirs: Bakken Application" SPE 161137 presented at SPE Canadian Unconventional Resources Conf., Calgary, Alberta, Canada (30 Oct-Nov1 2012)

W. Dershowitz, P. LaPointe, T. Eiben, and L. Wei: "Integration of Discrete Fracture Network Methods with Conventional Simulator Approaches," SPE Res. Eval. & Eng., 165-170, (April 2000).

L. Du, L. Chu "Understanding Anomalous Phase Behavior in Unconventional Oil Reservoirs", SPE 161830 presented at SPE Canadian Unconventional Resources Conf., Calgary, Alberta, Canada (30 Oct-Nov1 2012)

K. Esler, K. Mukundakrishnan, V. Natoli, J. Shumway, Y. Zhang and J. Gilman: “Realizing the Potential of GPUs for Reservoir Simulation” Mo A05 paper presented at ECMOR XIV, 14th European Conference on the Mathematics of Oil Recovery, Catania, Sicily, Italy, (8-11 September 2014)

J. LeFever "Williston Basin Correlation Cross-Section - Bakken Formation" Geologic Investigations Report GI-14 poster by North Dakota Geologic Survey (NDIC 2005)

J. Gilman, H. Wang, S. Fadaei, M. Uland: “A New Classification Plot for Naturally Fractured Reservoirs”, SPE 146580 prepared for presentation at the 2011 CSUG/SPE Unconventional Resources Conference, (Nov. 15-17, 2011), Alberta, Calgary, Canada

R. Michelena, K. Godbey, and H-Z. Meng “Flow simulation models for unconventional reservoirs: The role of seismic data”, SEG Technical Program Expanded Abstracts 2014: pp. 4427-4431 (2014)

K. Mukundakrishnan, K. Esler, D. Dembeck, V. Natoli, J. Shumway, Y. Zhang, J. Gilman, H. Meng: “Accelerating Tight Reservoir Workflows with GPUs”, SPE 173246 paper presented at the SPE Reservoir Simulation Symposium held in Houston, Texas, USA, (23-25 February 2015)

F. Perapon, B. Kurtoglu, H. Kazemi, S. Charoenwongsa, and Y-S. Wu,” The Effect of Osmotic Pressure on Improved Oil Recovery from Fractured Shale Formations” SPE 198998 presented at SPE Unconventional Resources Conference, Woodlands TX, (1-3 April 2014)

R. Weiss and J. Shragge, “Solving 3D anisotropic elastic wave equations on parallel GPU devices" published by Society of Exploration Geophysicists in GEOPHYSICS Vol. 78, No. 2, pp. F7-F15 (March 2013)